Supporting Information

Lanthanide Metal-Organic Frameworks for the Fixation of CO_2 Under Aqueous-rich and Mixed-gas Conditions

David H. Le[1], Ryan P. Loughan[1], Andrzej Gładysiak[2], Nakul Rampal,[3] Isabelle A. Brooks[1], Ah-Hyung Alissa Park[2], David Fairen-Jimenez,[3] Kyriakos C. Stylianou[1*]

[1]Materials Discovery Laboratory (MaD Lab), Department of Chemistry, Oregon State University, Corvallis, Oregon, United States, 97331

[2]Department of Earth and Environmental Engineering, Department of Chemical Engineering, Lenfest Center for Sustainable Energy, Columbia University, New York, United States

[3]Adsorption & Advanced Materials Laboratory (A^2ML), Department of Chemical Engineering & Biotechnology, University of Cambridge, Philippa Fawcett Drive, Cambridge CB3 0AS, UK

Email. kyriakos.stylianou@oregonstate.edu

Table of Contents

S1. Experimental 3
S1.1. Materials 3
S1.2. Synthetic Protocols 3
S1.2.1. Synthesis of Ln^{III}HTCPB MOF 3
S1.3. Characterization Protocols 3
S1.3.1. Thermogravimetric Analysis 3
S1.3.2. Powder X-Ray Diffraction 4
S1.3.4. Elemental Analysis 4
S1.3.3. Fourier Transform Infrared Spectroscopy 4
S1.3.4. Gas Sorption Measurements 4
S1.3.5. Variable-Gas TGA of Epoxide Loaded [Ce(HTCPB)] 5
S2. Characterization 6
S2.1. Thermogravimetric Analysis 6
S2.2. Powder X-ray Diffraction 7
S2.3. Fourier Transform Infrared Spectroscopy 8
S2.4. Elemental Analysis 9
S2.5. CO_2 Adsorption Isotherms 10
S2.6. Variable-Gas TGA of Epoxide Loaded [Ce(HTCPB)(PO)] 12
S2.7. Le Bail refinement of the [Ln(HTCPB)] PXRD 13
S3. Catalysis Experiments 16
S3.1. Catalytic Procedure 16
S3.2. NMR Spectra 17
S3.2.1 Qualification by ^{1}H NMR Spectroscopy 17
S3.2.2 Qualification by ^{13}C NMR Spectroscopy 18
S3.2.2 Quantification by ^{1}H NMR Spectroscopy 19
S4. Simulation Procedures 21
S5. Literature Comparison 26
S6. References 27

S1. Experimental

S1.1. Materials

All materials and chemicals used are detailed in this section. Propylene oxide (PO) (≥ 99%), 1,2-dimethoxyethane (DME) (99.5%), tetramethylammonium bromide (98%), 1,2,4,5-tetrakis(4-carboxyphenyl)benzene (H_4TCPB) (≥ 97%), cerium(III) nitrate hexahydrate (99%), neodymium(III) nitrate hexahydrate (99%), samarium(III) nitrate hexahydrate (99%), europium(III) nitrate hexahydrate (99%), terbium(III) nitrate hexahydrate (99%), dysprosium(III) nitrate hexahydrate (99%), ethanol (EtOH) (99.5%) and acetone were purchased from Sigma Aldrich. CO_2, CO_2/CH_4 and CO_2/N_2 mixed gases (≥ 99.99%) were supplied commercially by Airgas. All the above chemicals were used without further purification.

S1.2. Synthetic Protocols

S1.2.1. Synthesis of Ln^{III}HTCPB MOF

The metal-organic framework [Ln(HTCPB)(H_2O)(EtOH)]·guests (Ln = Ce, Nd, Sm, Eu, Tb, Dy) was synthesized following the procedure described by Warren et al. H_4TCPB (10 mg), $Ln(NO_3)_3 \cdot 6H_2O$ (20 mg), EtOH (3 mL), and DI H_2O (3 mL) were added to a 3 dram borosilicate vial and sealed.[1] The mixture was sonicated for 15 min then vortexed for 15 seconds to form an inert suspension. The mixture was heated in a 120 °C oven at 2.0 °C min^{-1} for 48 h and then cooled from 120 °C at 0.2 °C min^{-1} to room temperature. The resulting beige-white crystals were harvested by vacuum filtration and purified with a double treatment of EtOH followed by a double treatment of DI H_2O. The as-synthesized [Ln(HTCPB)(H_2O)(EtOH)]·guests was dried and activated under vacuum at 100 °C for 12 h to remove guest molecules to give rise to [Ln(HTCPB)] at 60-97% yield.

S1.3. Characterization Protocols

S1.3.1. Thermogravimetric Analysis

TGA was performed using a standard TG-DTA analyzer from Hiden Analytical. Each [Ln(HTCPB)] MOF was analyzed as-synthesized to evaluate thermal stability. Analysis was performed from 20 °C to 600 °C at a 5 °C min^{-1} ramp under 100 ml min^{-1} airflow.

S1.3.2. Powder X-Ray Diffraction

Phase purity and crystallinity of the [Ln(HTCPB)] were confirmed by PXRD in a Rigaku Miniflex 600 diffractometer (monochromated Cu Kα radiation, λ = 1.54178 Å). The samples were collected for 2θ range of 3 – 35 degrees at a scan rate of 0.075 degrees min^{-1} with 0.02 degree step size at ambient conditions. All collected diffraction patterns (Figures S2a-2f) were compared to calculated peaks for [Ce(HTCPB)] generated from known crystallography data. The relatively similar peaks obtained from the synthesized material confirmed the successful synthesis of the MOFs.

S1.3.3. Elemental Analysis

Elemental analysis was performed on the activated [Ln(HTCPB)]. All measurements were performed at ambient conditions and the results have been detailed in Table S1.

S1.3.4. Fourier Transform Infrared Spectroscopy

All FT-IR measurements were performed for each [Ln(HTCPB)] on a Perkin Elmer Spectrum Two Spectrometer equipped with a $LiTaO_3$ MIR detector. The coordination of the carboxylate groups of H_4TCPB with the Ln atoms causes electron delocalization via hyperconjugation resulting in red shifting. The obtained spectra of the MOFs were compared to that of H_4TCPB to confirm ligand and metal ion incorporation into the framework by a red shift.

S1.3.5. Gas Sorption Measurements

N_2 sorption isotherms on [Ce(HTCPB)] were collected using a 3FLEX Adsorption Analyzer from Micrometrics. A ~50 mg sample of [Ce(HTCPB)] was outgassed at 140 °C overnight. For Brunauer-Emmett-Teller (BET) area measurements, the measured sample was chilled to 77 K in a Dewar vessel containing liquid nitrogen then had uptake measurements to an absolute pressure of 1 atm. [Ce(HTCPB)] showed a BET area of 198 m^2 g^{-1} which is consistent with values reported in literature.[1] CO_2 sorption isotherms were also collected to assess CO_2 uptake capacity up to 760 mmHg absolute at room temperature. Samples for CO_2 isotherm adsorption measurements were prepared in the same way as for N_2 isotherms. For these measurements, the absolute uptake of CO_2 was determined for each material as detailed in Table S2.

S1.3.6. Variable-Gas TGA of Epoxide Loaded [Ce(HTCPB)]

To evaluate the effects of loading [Ce(HTCPB)] with propylene oxide, variable-gas TGA was performed in the presence of alternating cycles of N_2 and CO_2 atmospheres using a Labsys Evo TG DTA DSC instrument at 1 bar.

For the unloaded [Ce(HTCPB)], an alumina crucible was charged with 30 mg of crystalline powder of [Ce(HTCPB)] and loaded onto the TGA instrument. The sample was heated in the stream of N_2 flowing at 50 mL min^{-1} to 150 °C at the rate of 10 °C min^{-1}, then kept at 150 °C for 60 min, cooled down to 25 °C at the rate of 5 °C min^{-1}, and kept at 25 °C for 30 min. The gas was switched to CO_2 flowing at 50 mL min^{-1} for 60 min. Then, the gas was switched back to N_2, and the 25–150–25 °C temperature swing was repeated. The mass was recorded thoughout the entire experiment and corrected for gas buoyancy using the blank measurement. The CO_2 uptake capacity was calculated assuming that the mass just before switching gas to CO_2 corresponds to the fully activated material, while the subsequent increase of mass is only due to CO_2 adsorption.

For the propylene oxide-loaded [Ce(HTCPB)], in order not to remove the propylene oxide from within the pores of the material, the CO_2 working capacity measurement was performed isothermally at 25 °C. The sample was first stabilized in the stream of N_2 (50 mL min^{-1}) for 30 min, then exposed to CO_2 (50 mL min^{-1}) for 60 min, and finally back to N_2 (50 mL min^{-1}) for 90 min. The CO_2 working capacity was calculated analogously to that of [Ce(HTCPB)].

The [Ce(HTCPB)] showed a CO_2 uptake capacity of 1.4 mmol g^{-1} which is consistent with the in-house measurements shown in Table S2. Upon loading with propylene oxide, the uptake capacity decreased to 0.32 mmol g^{-1}. While the binding of epoxide to the Ce^{III} active sites reduces the accessible pore volume by 77%, there is still accessible free volume for CO_2 to be captured within the pores. This means that interactions between captured CO_2 and bonded epoxides can occur within the pore channels of the [Ce(HTCPB)] and catalysis is possible.

S2. Characterization

S2.1. Thermogravimetric Analysis

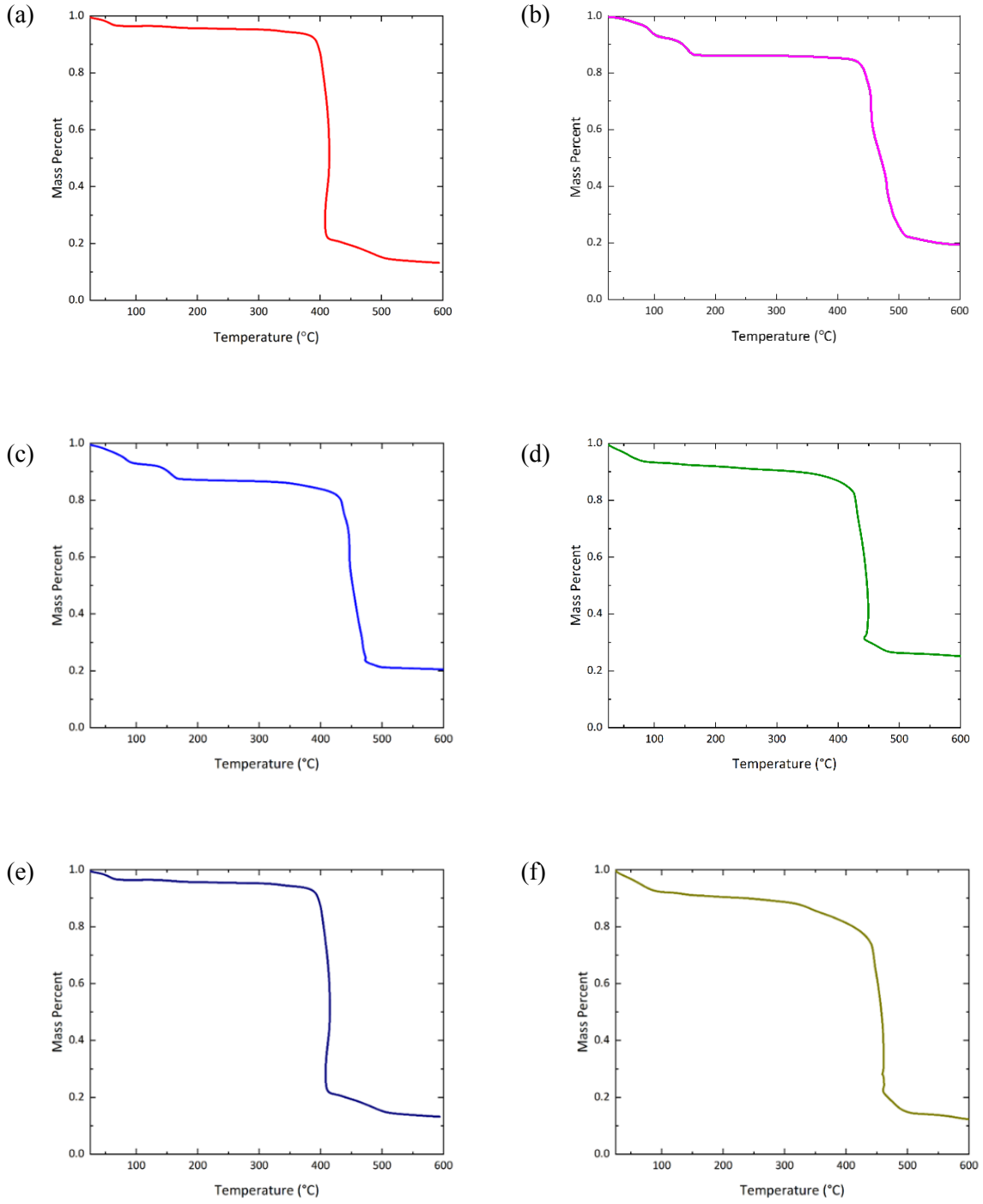

Figure S1a-f. TGA plots of Ln^{III}HTCPB (Ln = Ce (a), Nd (b), Sm (c), Eu (d), Tb (e), Dy (f)).

S2.2. Powder X-ray Diffraction

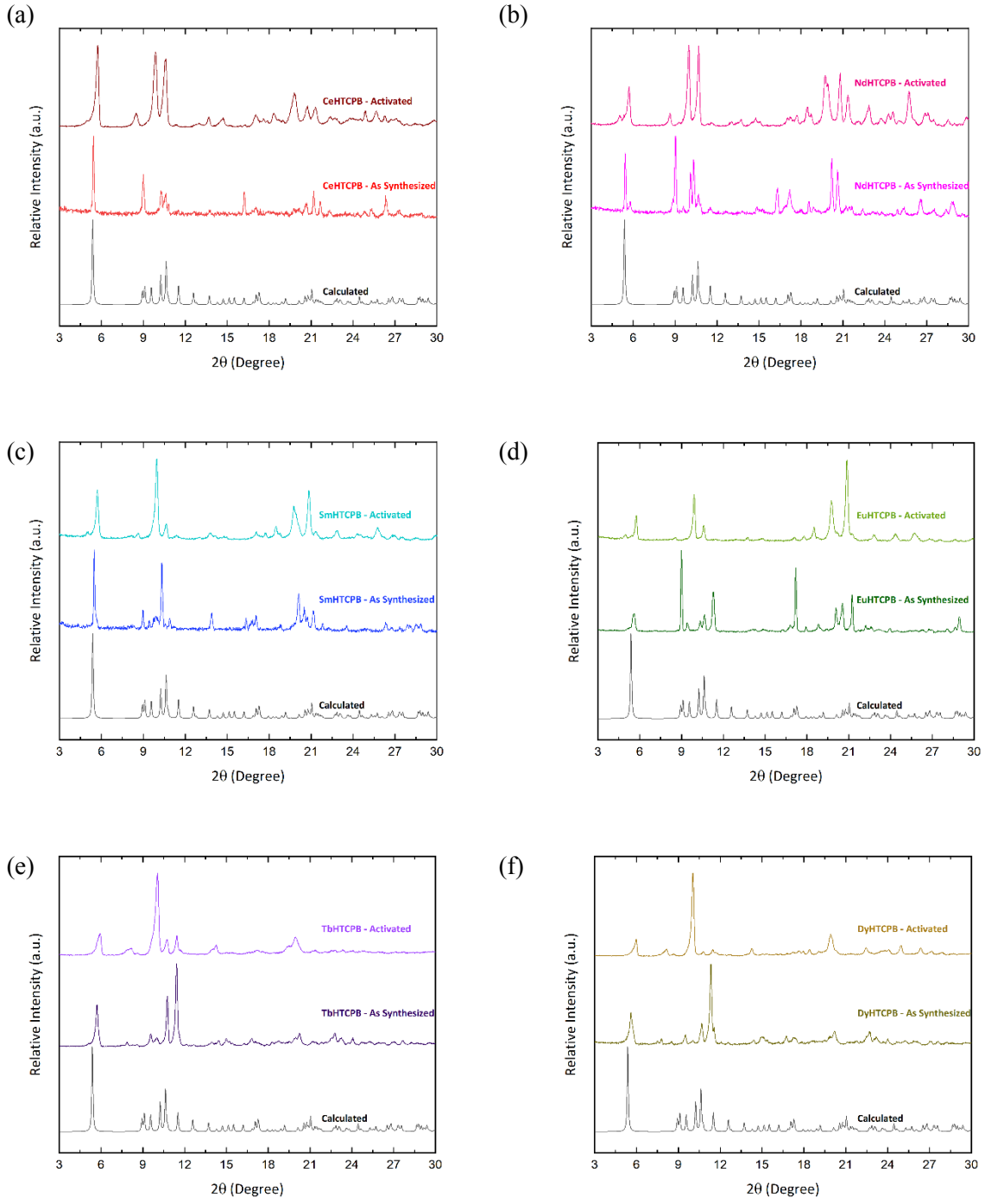

Figure S2a-f. PXRD plots of $Ln^{III}HTCPB$ (Ln = Ce, Nd, Sm, Eu, Tb, Dy) compared to calculated peaks from crystallography data. Activated material refers to material after CO_2 at 298 K sorption measurements.

S2.3. Fourier Transform Infrared Spectroscopy

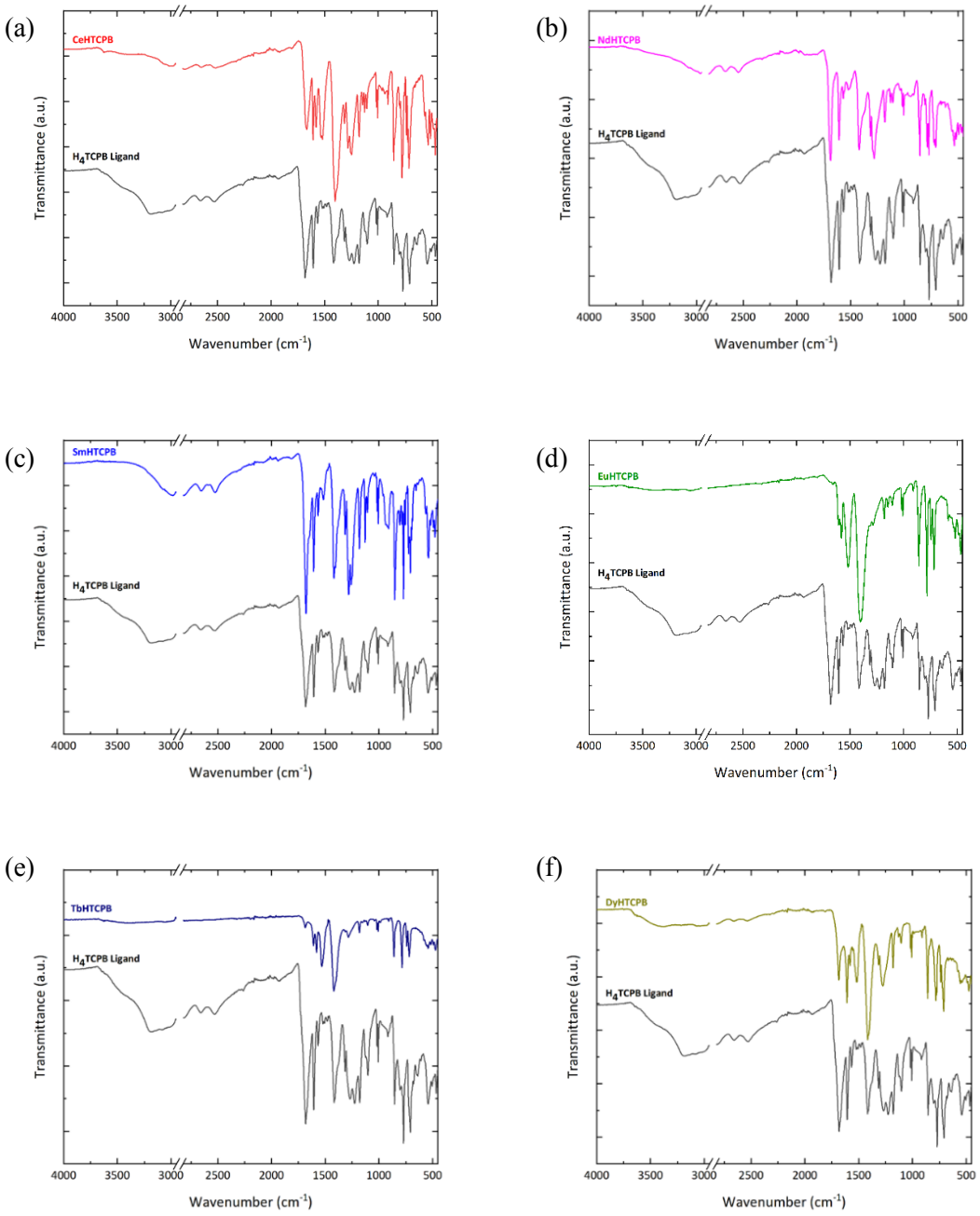

Figure S3a-f. FTIR plots of Ln^{III}HTCPB (Ln = Ce, Nd, Sm, Eu, Tb, Dy).

S2.4. Elemental Analysis

Table S1. Elemental analysis of [Ln(HTCPB)]. The water content in the samples prepared for CHN analysis most likely arises from adventitious contamination by atmospheric water incurred during analysis.

Material	Formula	Elements	Theory	Found
Ce(HTCPB)	$[Ce(HTCPB)]\cdot(H_2O)_{1.0}$	C	57.22	57.18
		H	2.97	3.01
Nd(HTCPB)	$[Nd(HTCPB)]\cdot(H_2O)_{0.7}$	C	57.33	57.33
		H	2.89	3.05
Sm(HTCPB)	$[Sm(HTCPB)]\cdot(H_2O)_{0.3}$	C	57.41	57.33
		H	2.78	2.89
Eu(HTCPB)	$[Eu(HTCPB)]\cdot(H_2O)_{1.1}$	C	56.15	56.01
		H	2.94	2.99
Tb(HTCPB)	$[Tb(HTCPB)]\cdot(H_2O)_{1.4}$	C	55.21	55.01
		H	2.97	2.98
Dy(HTCPB)	$[Dy(HTCPB)]\cdot(H_2O)_{0.8}$	C	55.76	55.75
		H	2.84	3.05

S2.5. CO_2 Adsorption Isotherms

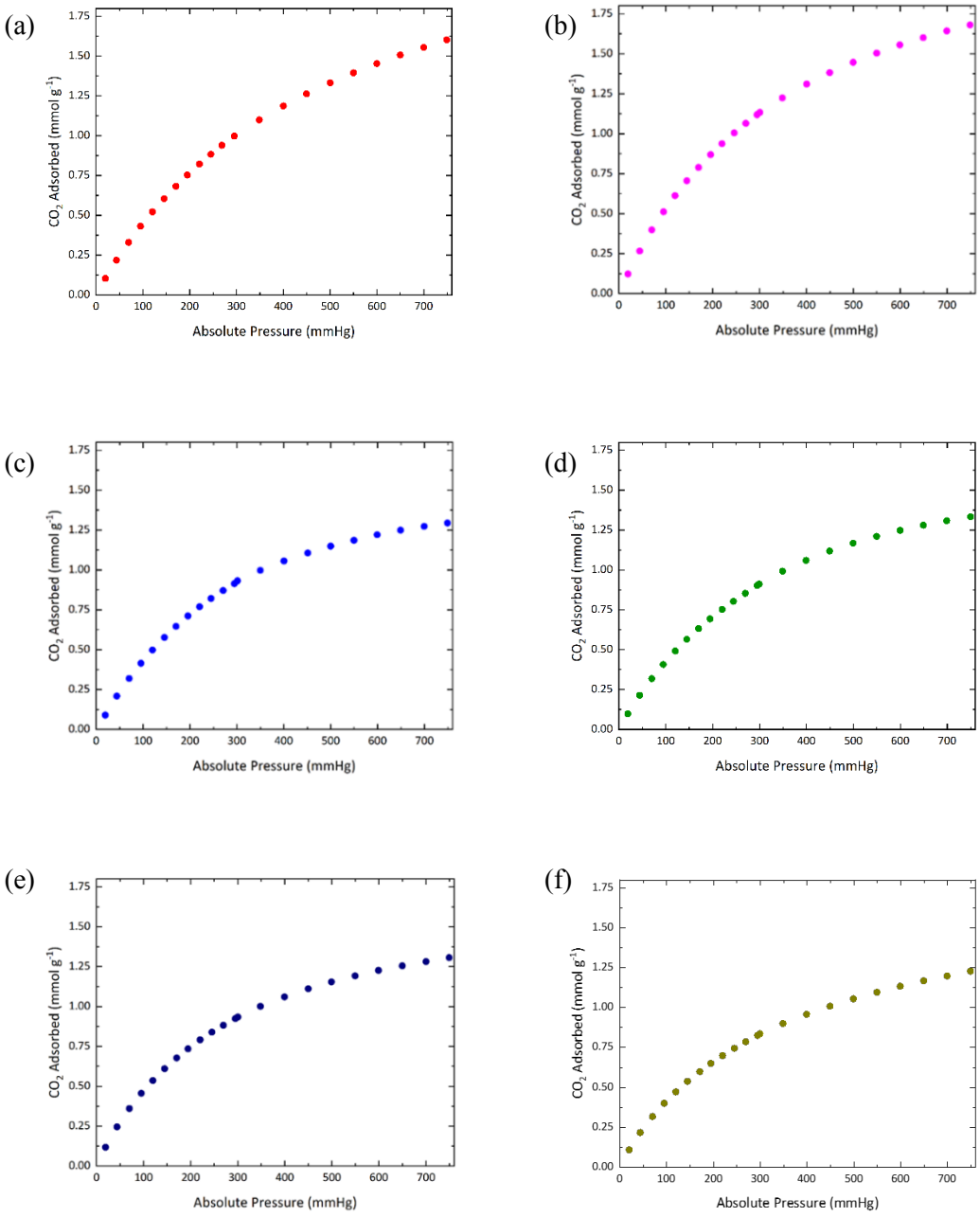

Figure S4a-f. CO_2 adsorption isotherm at 298 K plots for [Ln(HTCPB)] (Ln = Ce (a), Nd (b), Sm (c), Eu (d), Tb (e), Dy (f)).

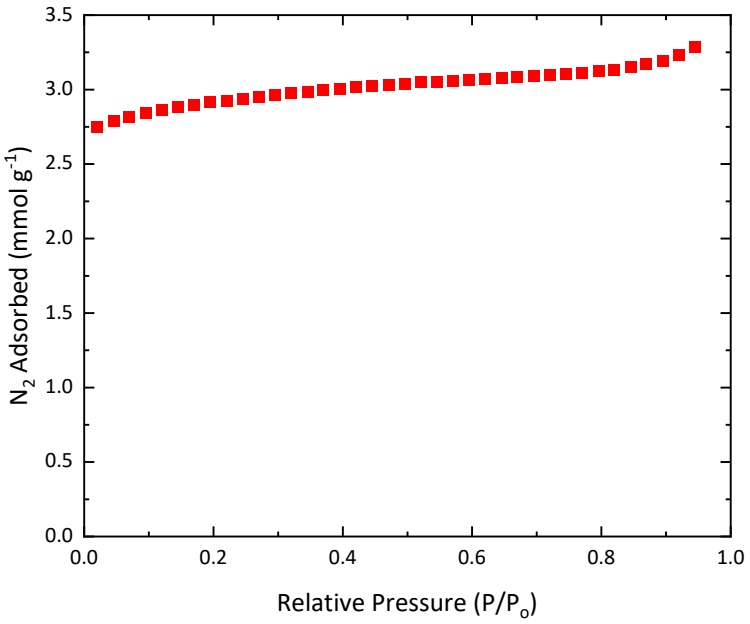

Figure S5. N_2 adsorption isotherm at 77 K plot for [Ce(HTCPB)].

Table S2. CO_2 uptake for each [Ln(HTCPB)] collected at 298 K and 760 mmHg.

#	Ln	CO_2 Uptake Capacity [mmol g^{-1}]
58	Ce	1.60
60	Nd	1.68
62	Sm	1.29
63	Eu	1.33
65	Tb	1.31
66	Dy	1.24

S2.6. Variable-Gas TGA of Epoxide Loaded [Ce(HTCPB)(PO)]

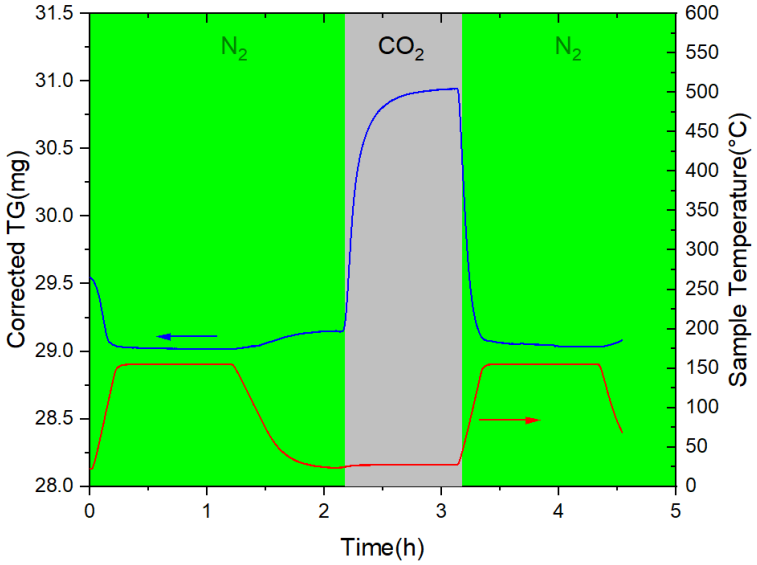

Figure S6. Variable-gas TGA of [Ce(HTCPB)] after activation.

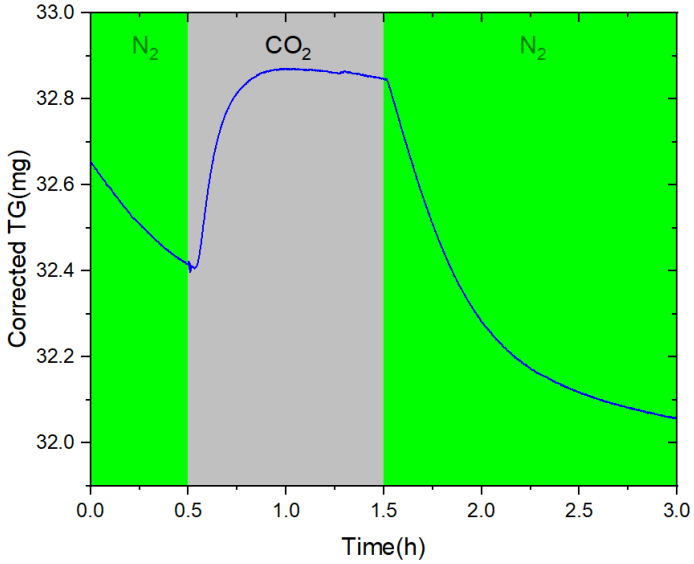

Figure S7. Variable-gas TGA of propylene oxide-loaded [Ce(HTCPB)(PO)] collected at 298 K.

Table S3. CO_2 uptake capacity derived from temperature-swing TGA collcted at 298 K.

Material	CO_2 Uptake Capacity [mmol g^{-1}]
Un-Loaded CeHTCPB	1.40
Epoxide-Loaded CeHTCPB	0.32

S2.7. Le Bail refinement of the [Ln(HTCPB)] PXRD

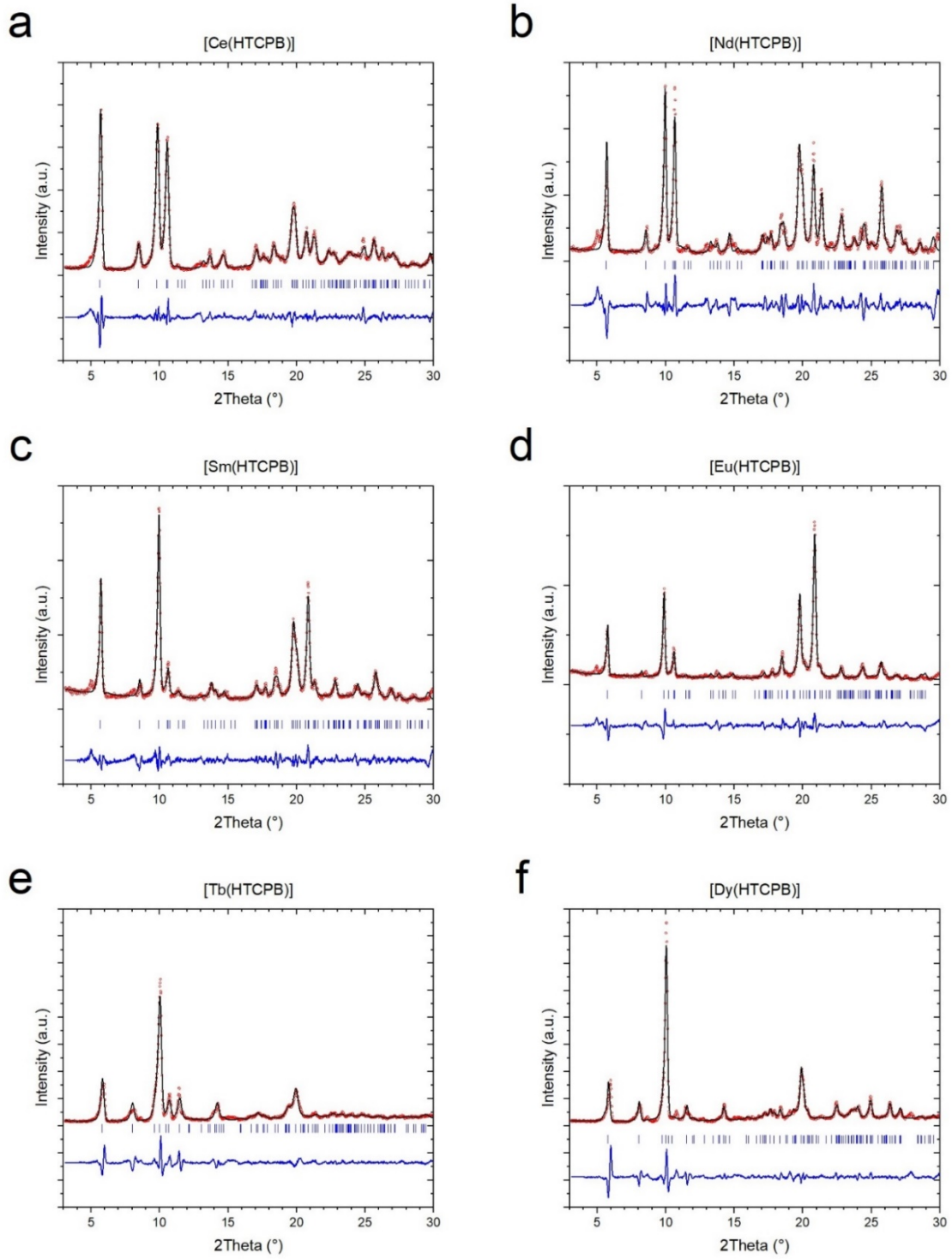

Figure S8. Le Bail refinement of the [Ln(HTCPB)] PXRD patterns. The associated fitting parameters are listed in Table S4.

Table S4. Unit-cell parameters a, b, c, α, β, γ, unit-cell volume V, and fitting figures of merit R_p, R_{wp}, and R_{exp} derived from the Le Bail refinement of the [Ln(HTCPB)] PXRD patterns. Data compared to the previously published crystal strcutures. All unit cells are of $P\bar{1}$ space-group symmetry.

MOF	a [Å]	b [Å]	c [Å]	α [°]	β [°]	γ [°]	V [Å^3]	R_p [%]	R_{wp} [%]	R_{exp} [%]
[Ce(HTCPB)]	8.966(2)	10.815(2)	16.215(5)	81.75(2)	73.73(2)	74.79(2)	1452.0(6)	8.43	12.0	4.53
[Nd(HTCPB)]	8.950(2)	10.834(2)	16.277(7)	82.15(2)	73.93(2)	73.74(2)	1452.7(8)	14.2	19.9	5.36
[Sm(HTCPB)]	8.941(2)	10.805(2)	16.163(7)	82.15(2)	74.27(2)	74.00(2)	1441.1(8)	8.90	12.0	5.86
[Eu(HTCPB)]	8.970(2)	11.152(3)	16.075(7)	83.97(2)	74.04(2)	75.08(4)	1476.0(9)	11.4	15.5	6.11
[Tb(HTCPB)]	8.940(8)	11.417(8)	16.130(12)	85.60(4)	75.94(8)	80.45(12)	1573(5)	10.9	15.2	4.74
[Dy(HTCPB)]	9.093(2)	11.234(6)	15.887(8)	86.08(4)	75.99(3)	80.31(3)	1551.4(12)	12.5	18.6	4.68
[Nd(HTCPB)]	9.3093(11)	11.9578(14)	15.8071(19)	81.178(4)	73.671(4)	71.162(4)	1594.4(3)	Previously reported structure[1]		
[Ce(HTCPB)]	9.2989(11)	11.4163(13)	15.2492(17)	93.756(5)	90.263(6)	93.814(6)	1611.7(3)	Previously reported structure[1]		

Experimental. Le Bail refinement of the powder XRD patterns of [Ln(HTCPB)] was performed using the program FullProf version 7.40.[2] Previously published unit-cell parameters of [Ce(HTCPB)][1] adjusted manually served as a starting point of the refinement. Background was fixed using a set of points, while the peaks were fitted to the pseudo-Voigt function. The fitting parameters included unit-cell parameters a, b, c, α, β, γ, Cagliotti parameters U, V, W, the shape parameter η_0, asymmetry parameters Asym1 and Asym2, and the instrumental zero.

S2.8. Powder X-ray Diffraction of Recycled [Ce(HTCPB)]

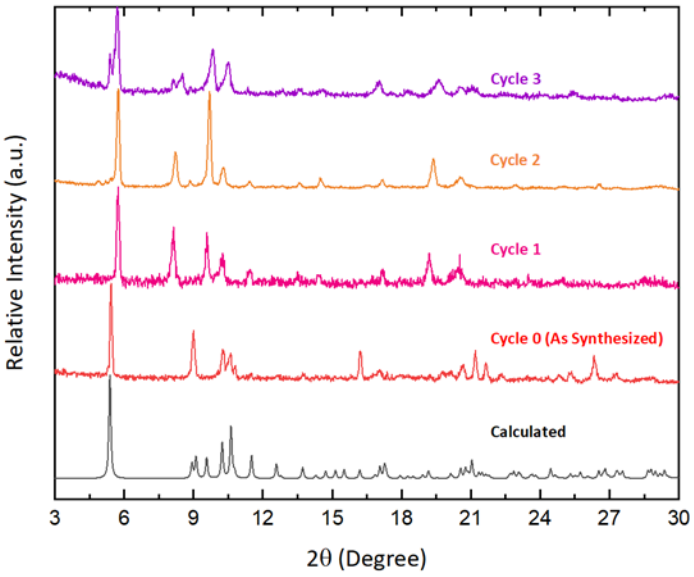

Figure S9. PXRD patterns of [Ce(HTCPB)] after catalysis.

S3. Catalysis Experiments

S3.1. Catalytic Procedure

[Ln(HTCPB)] (0.0145 mmol), tetramethylammonium bromide (100.0 mg, 0.310 mmol), 1,2-dimethyoxyethane (1.75 mL, 16.9 mmol), and propylene oxide (0.25 mL, 3.57 mmol) were added to a 25 mL stainless steel autoclave reactor (Parr Instruments Series 4790). The reactor was pressurized with 10 bars of pure CO_2 before heating to a sustained 100 °C for 12 hours. After 12 hours, the reactor was cooled down to room temperature in a refrigerated water bath for 20 min and depressurized.

A 25 μL aliquot was taken from the reaction solution for ^1H NMR analysis to determine propylene oxide conversion. The remaining solution was then vacuum filtered to recover the catalyst which was then sequentially washed with double treatments of acetone and then a double treatment of DI H_2O. The recovered catalyst was then vacuum dried overnight to be used for the next cycle.

S3.2. NMR Spectra

S3.2.1 Qualification by ^{1}H NMR Spectroscopy

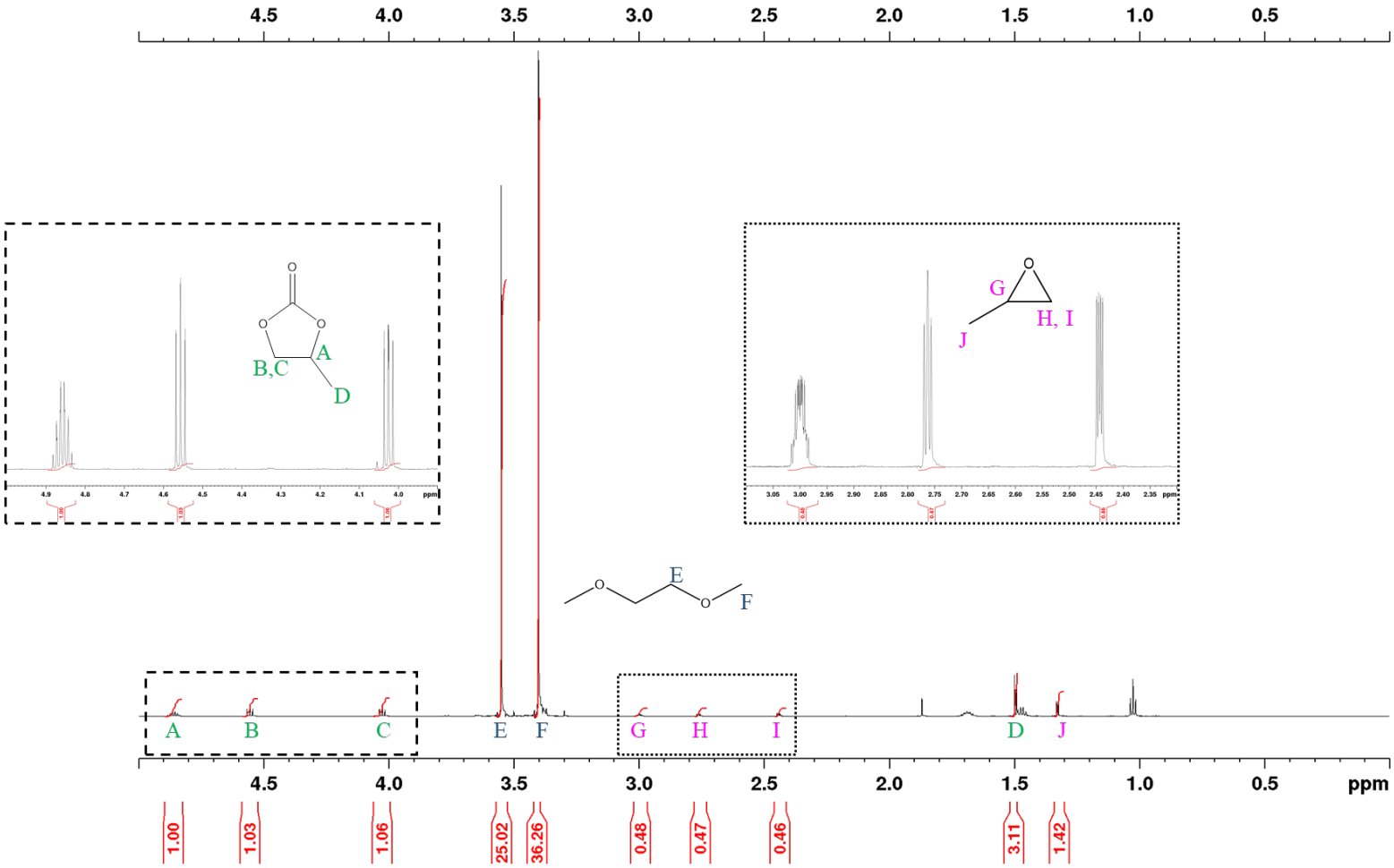

Figure S10. ^{1}H NMR ($CDCl_3$, 500 MHz) spectra showing peaks of propylene oxide (magenta), propylene carbonate (green), and DME (blue). All other residual peaks are due to TBAB (unlabeled).

S3.2.2 Qualification by ^{13}C NMR Spectroscopy

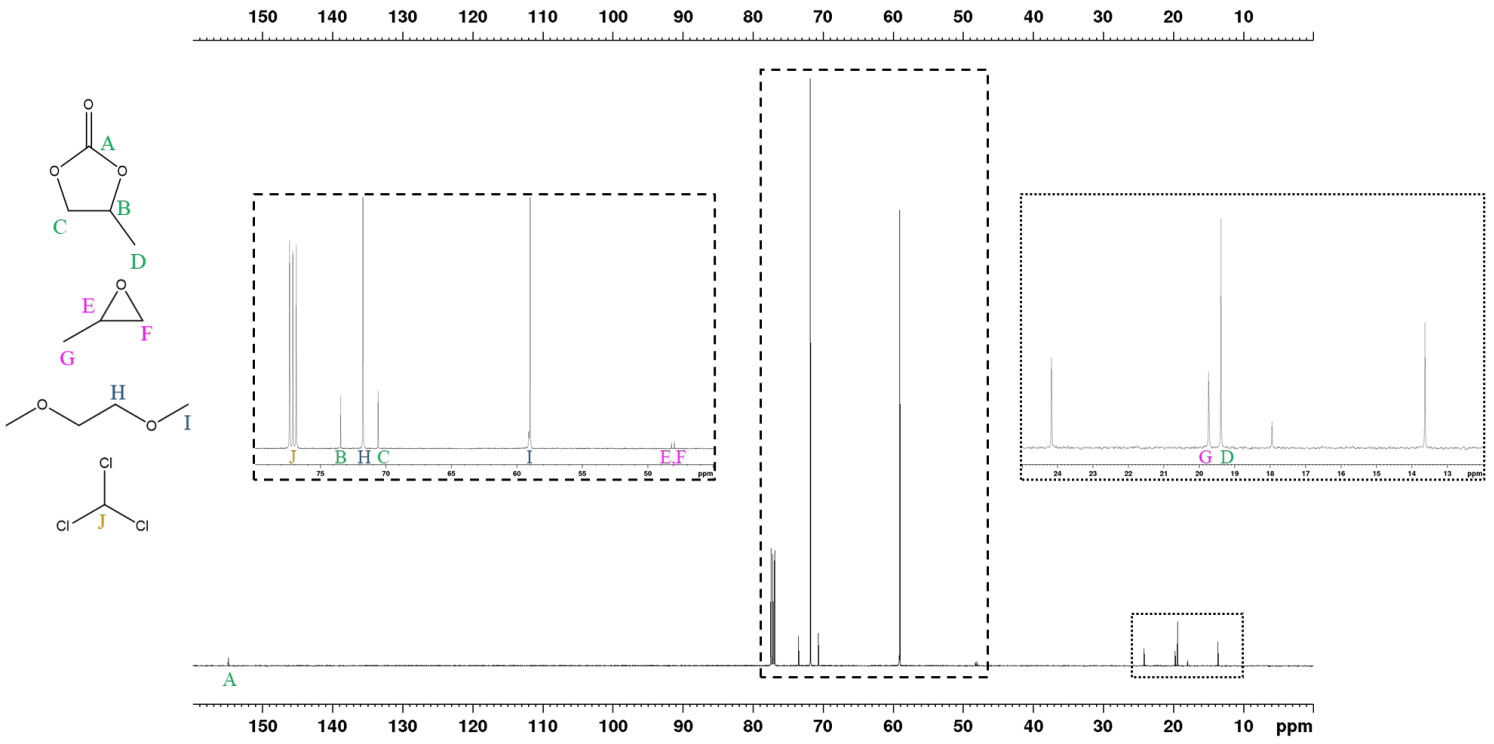

Figure S11. ^{13}C NMR ($CDCl_3$, 500 MHz) spectra showing peaks of propylene oxide (magenta), propylene carbonate (green), and DME (blue). All other residual peaks are due to TBAB (unlabeled) and chloroform (I).

S3.2.2 Quantification by ^{1}H NMR Spectroscopy

The yield of propylene carbonate was determined by ^{1}H NMR. A 25 µL aliquot was taken from the reaction solution and diluted with 580 µL of deuterated chloroform in a standard 5 mm NMR tube. NMR spectra were recorded with a 500 MHz Bruker Avance 500 equipped with a BBO probe.

To calculate the yield, the ring protons of propylene carbonate and the protons of 1,2-dimethoxyethane (DME) were considered for the following calculations. Sample calculations shown below are in reference to data from Figure S10. First, the ratio of propylene carbonate to DME was calculated from area integrals obtained by NMR.

$$\frac{\boldsymbol{M_{Carbonate}}}{\boldsymbol{M_{DME}}} = \left(\frac{I_{Carbonate}}{I_{DME}}\right)\left(\frac{N_{DME}}{N_{Carbonate}}\right) = \left(\frac{3.02}{48.99}\right)\left(\frac{10}{3}\right) = 0.205$$

- I = Integral Area
- N = Number of Nuclei
- M = Number of Moles

As a solvent, the molar amount of DME (16.9 mmol) was constant throughout the entire reaction. Using the initial molar amount of DME used for the reaction, the total molar amount of propylene carbonate was calculated.

$$\boldsymbol{M_{Carbonate,Total}} = \left(\frac{M_{Carbonate}}{M_{DME}}\right)\left(M_{DME,Total}\right) = (0.205)(16.9\ \text{mmol}) = 3.4645\ \text{mmol}$$

The yield of propylene carbonate is then calculated by comparison to the original molar amount of PO added (3.57 mmol).

$$\boldsymbol{Yield} = \left(\frac{M_{Carbonate,Total}}{M_{PO}}\right)(100\%) = \left(\frac{3.4645\ \text{mmol}}{3.57\ \text{mmol}}\right)(100\%) = \boxed{\mathbf{97.0\%}}$$

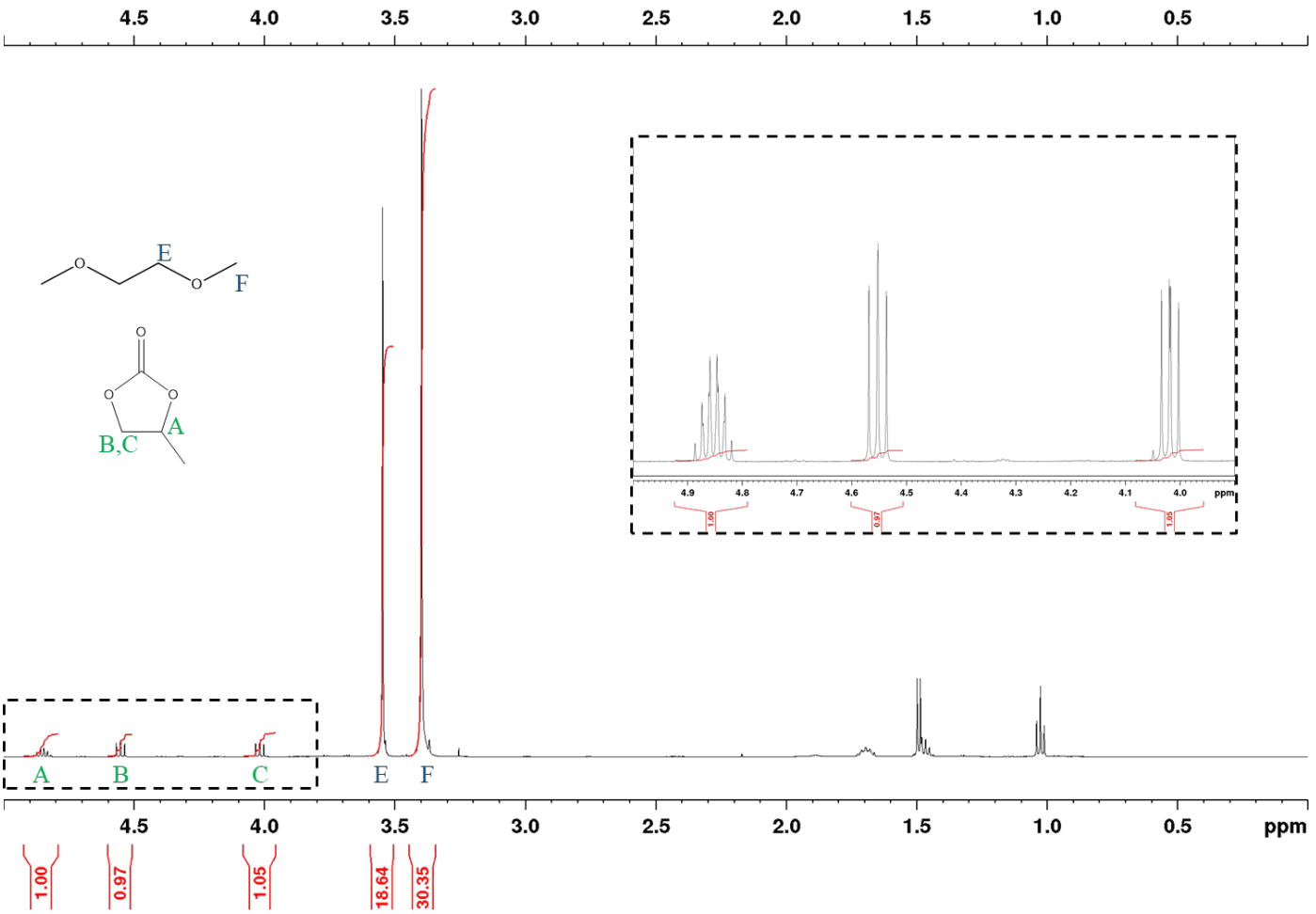

Figure S12. ^{1}H NMR ($CDCl_3$, 500 MHz) spectra showing peaks of propylene carbonate (green) and DME (blue) which were used to calculate the yield of propylene carbonate. Only the peaks of the ring protons of propylene carbonate (3H total) were considered as the methyl peaks overlapped with peaks of the TBAB.

S4. Simulation Procedures

S4.1 Grand Canonical Monte-Carlo (GCMC) Simulations

CO_2 adsorption at 298 K was simulated using the Grand Canonical Monte Carlo method as implemented in the RASPA simulation package.[3] Monte Carlo moves consist of translation, insertion, deletion, and rotation moves, all taking place with equal probabilities. A total of 20,000 cycles for equilibration + an additional 20,000 cycles to average the properties are run. A cycle is defined as the maximum of 20 steps or the total number of molecules in the system; this means that on an average a Monte Carlo move has been attempted on each molecule in every cycle. The crystallographic information files (cif) for [Nd(HTCPB)], [Sm(HTCPB)], [Eu(HTCPB)], [Tb(HTCPB)], and [Dy(HTCPB)], have been created by replacing the metal atom from the isostructural [Ce(HTCPB)], followed by geometric optimization of the framework using the Forcite module in Material Studio. The cif file for [Ce(HTCPB)] has been taken from the Cambridge Structural Database (CSD), CSD Refcode: FOFCUA.[4] For all the structures, periodic boundary conditions are applied in all directions to make sure that a distance of at least twice the cutoff radius is maintained between the periodic images. Intermolecular interactions are modeled using the Lennard-Jones (LJ) potential with a cutoff of 12.8 Å. Lorentz-Berthelot mixing rules are used for all the cross interaction terms. Electrostatic interactions are modeled using the coulombic potential and are computed using the Ewald summation method with the precision set to 10^{-6}. The partial charges for the framework are calculated using the EQeq protocol.[5] The framework atoms are modeled using LJ parameters taken from a combination of the DREIDING force field for the C, H, and O atoms, and the Universal force field (UFF), for the Ce, Nd, Sm, Eu, Tb, and Dy atoms.[6, 7] Table S5 lists the LJ parameters used for the framework atoms. CO_2 is modeled as a rigid molecule with the LJ parameters, and charges taken from the TraPPE force field.[8] Table S6 lists the LJ parameters and charges for the CO_2 molecule.

S4.2 Energy Decomposition Analysis (EDA)

EDA based on molecular force fields was performed using the Multiwfn package.[9] Here, it is important to point out that though other more accurate wavefunction based methods for energy decomposition exist, they are often too expensive for large systems. This problem is further exacerbated when working with heavy transition metals or lanthanides.

The total interaction energy between atom i and atom j can be decomposed into the following terms:

i) the van der Waals interaction energy (eq. 1), modeled using the Lennard-Jones (LJ) potential and consisting of two parts: the r^{12} term, which is the repulsive term and describes the Pauli repulsion at short ranges due to overlapping electron orbitals, and, the r^6 term, which is the long-range term describing the attraction (dispersion forces) at long ranges,

$$E_{ij}^{van\ der\ Waals} = E_{ij}^{repulsion} + E_{ij}^{dispersion} \qquad [1]$$

where

$$E_{ij}^{repulsion} = 4\varepsilon_{ij}\left(\frac{\sigma_{ij}}{r_{ij}}\right)^{12} \text{ and } E_{ij}^{dispersion} = -4\varepsilon_{ij}\left(\frac{\sigma_{ij}}{r_{ij}}\right)^{6} \qquad [2]$$

where, σ_{ij} is the distance at which the intermolecular potential between the two particles is zero, ε_{ij} is the depth of the potential well, and r_{ij} is the distance between atom i and atom j;

ii) and the electrostatic interaction energy, which is modeled using the coulombic potential (eq. 3),

$$E_{ij}^{electrostatic} = \frac{q_i q_j}{r_{ij}} \qquad [3]$$

where q is the atomic charge, subscripts indicate atom i or atom j, and r_{ij} is as described above. All the atoms in the system are modeled using LJ parameters taken from Universal Force Field (UFF) and are given in Table S5**.** [7] The mixing rules used here are as follows:

$$\varepsilon_{ij} = \sqrt{\varepsilon_i \varepsilon_j} \text{ and } \sigma_{ij} = \sqrt{\sigma_i \sigma_j}$$

where ε and σ are the LJ parameters (as described above) and the subscripts indicate atom i and atom j. The charges for all the atoms in the system are calculated using the EQeq protocol.[5]

Table S5. Lennard Jones parameters for the atoms used in the GCMC simulations/EDA. Column 1 lists the atom type; Columns 2 (σ in Å) and 3 (ε/K_b in K) list the LJ parameters taken from the DREIDING force field, and Columns 4 (σ in Å) and 5 (ε/K_b in K) list the LJ parameters taken from the UFF.

Atom	DREIDING LJ Parameters		UFF LJ Parameters	
	σ (Å)	**ε/kB (K)**	**σ (Å)**	**ε/kB**
C	3.473	47.888	3.431	52.873
H	2.846	7.654	2.571	22.156
O	3.033	48.190	3.118	30.213
Ce	-	-	3.168	6.546
Nd	-	-	3.185	5.036
Sm	-	-	3.136	4.028
Eu	-	-	3.112	4.028
Tb	-	-	3.074	3.525
Dy	-	-	3.054	3.525

Table S6. Lennard Jones parameters and charges for CO_2. Column 1 lists the atom type; columns 2, 3 and 4 list their corresponding LJ parameters and charges, σ in Å, ε/K_b in K, and q in e taken from the TraPPE force field [8].

Atom	LJ Parameters		q (e)
	σ (Å)	**ε/k_B (K)**	
C	2.80	27	0.70
O	3.05	79	-0.35
O	3.05	79	-0.35

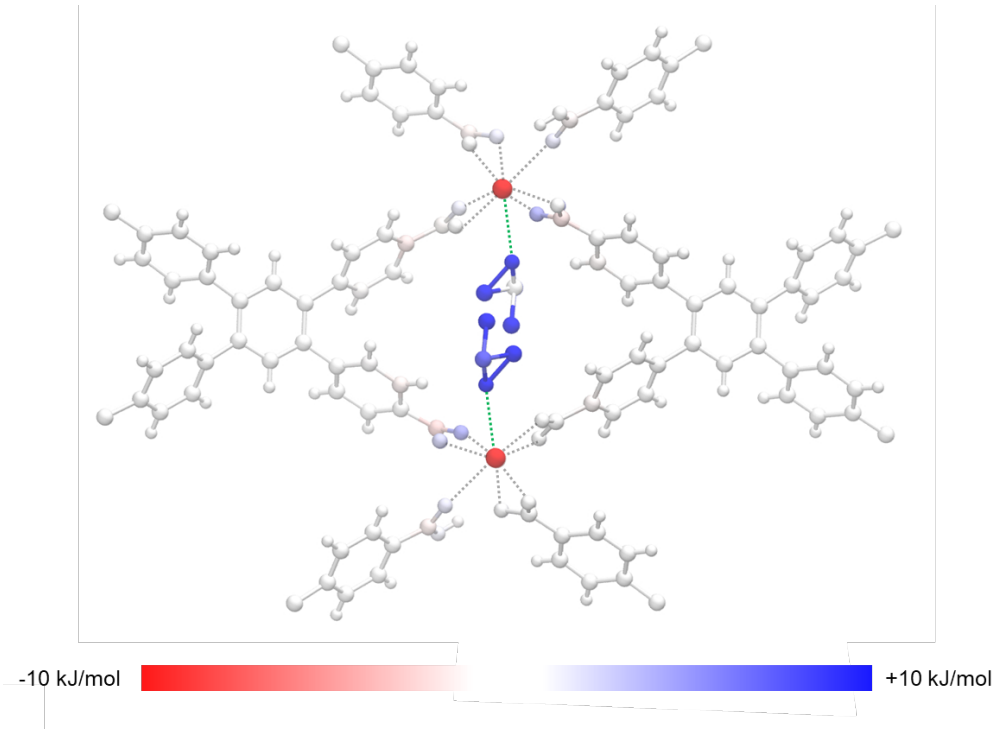

Figure S13. Energy decomposition analysis (EDA) for the [Ce(HTCPB)]-propylene oxide system. The atoms of the framework and the epoxide have been shaded based on the color scale, in which an interaction which has a positive contribution (repulsive) to the total interaction energy is shaded in blue whereas an interaction which has a negative contribution (attractive) to the total interaction energy is shaded in red, and white represents an interaction which has ~zero contribution to the total interaction energy. Any interaction greater than +10 kJ/mol is colored in blue, and any interaction less than ~10 kJ/mol is colored in red.

S4.3 Topographic Steric Map Calculation

The topographic steric maps are obtained using the SambVca 2 web application.[10] To build the topographic steric maps of the catalytic pocket, the framework-epoxide adduct was oriented in a Cartesian frame with the Ln atom selected as the origin. Next, a second point along the *z*-axis, and a third point along the *xz*-plane is selected. The environment around the Ln atom is evaluated in a region represented using a sphere of radius 3.5 Å, and a mesh of 0.1 Å is used to scan the sphere for buried voxels. The radii of the different atoms have been scaled by 1.17 and the hydrogen atoms are taken into account when building the steric map.[11] Table S7 lists the radii of the different atoms.

Table S7. Radii of the atoms used for the calculation of the topographic steric maps. Column 1 lists the atom type with the corresponding radii in Å (scaled by 1.17) given in Column 2.

Atom	Radii (Å)
C	1.99
H	1.28
O	1.78
Ce	2.83
Nd	2.80
Sm	2.76
Eu	2.75
Tb	2.73
Dy	2.70

S5. Literature Comparison

Table S8. Comparison of other materials reported using TBAB coupled PO to PC conversion.

Material	Temperature [°C]	CO_2 Pressure [bar]	Time [hr]	TOF [hr^{-1}]	Yield [%]	Reference
MMCF-2	25	1	48	5.3	95.4	12
MOF-505	25	1	48	4	48.8	12
HKUST-1	25	1	48	4.1	49.2	12
MMPF-9	25	1	48	14.6	87.4	13
USTC-253-TFA	25	1	72	1.2	81.3	14
MIL-101(Cr)	25	8	24	10.3	82.0	15
Ba-(BDPO)	25	10	48	4.1	99.2	16
MOF-5	50	60	4	36.4	94.5	17
TbL	70	10	12	2.4	45.5	18
SmBTB	80	1	15	12.1	100	19
Cu_2BPDSDC	80	25	5	19.1	99.0	20
Zeolite-β	120	7	3	16.0	100	21
UMCM-1-NH_2	120	12	24	5.9	91.0	22
NH_2-MIL-101(Al)	120	18	6	21.7	96.0	23
[Ce(HTCPB)]	100	2	12	13.4	65.4	This Work
[Ce(HTCPB)]	100	10	12	20.0	99.5	This Work

Table S9. Comparison of other materials reported using PO to PC conversion in mixed gas.

Material	N_2/CO_2 Ratio	Temperature [°C]	CO_2 Pressure [bar]	Time [hr]	TOF [hr^{-1}]	Yield [%]	Reference
BpZn@MA – mesoporous organic polymer	80/20	100	4	6	1580	99.0	24
$ZrCl_4(OEt_2)_2$ – zirconium alkyl complex	85/15	60	1	18	1.69	9.9	25
Zn(Py)(Atz) – MOF	85/15	60	1	24	1.92	29.0	26
[Ce(HTCPB)] – MOF	80/20	100	2	12	13.32	65.4	This Work

S6. References

1. J. E. Warren, C. G. Perkins, K. E. Jelfs, P. Boldrin, P. A. Chater, G. J. Miller, T. D. Manning, M. E. Briggs, K. C. Stylianou, J. B. Claridge and M. J. Rosseinsky, *Angew Chem Int Edit*, 2014, **53**, 4592-4596.
2. J. Rodríguez-Carvajal, *Physica B: Condensed Matter*, 1993, **192**, 55-69.
3. D. Dubbeldam, S. Calero, D. E. Ellis and R. Q. Snurr, *Mol Simulat*, 2016, **42**, 81-101.
4. P. Z. Moghadam, A. Li, S. B. Wiggin, A. Tao, A. G. P. Maloney, P. A. Wood, S. C. Ward and D. Fairen-Jimenez, *Chemistry of Materials*, 2017, **29**, 2618-2625.
5. C. E. Wilmer, K. C. Kim and R. Q. Snurr, *J Phys Chem Lett*, 2012, **3**, 2506-2511.
6. S. L. Mayo, B. D. Olafson and W. A. Goddard, *Journal of Physical chemistry*, 1990, **94**, 8897-8909.
7. A. K. Rappé, C. J. Casewit, K. Colwell, W. Goddard Iii and W. Skiff, *Journal of the American chemical society*, 1992, **114**, 10024-10035.
8. J. J. Potoff and J. I. Siepmann, *Aiche J*, 2001, **47**, 1676-1682.
9. T. Lu and F. Chen, *J Comput Chem*, 2012, **33**, 580-592.
10. L. Falivene, R. Credendino, A. Poater, A. Petta, L. Serra, R. Oliva, V. Scarano and L. Cavallo, *Organometallics*, 2016, **35**, 2286-2293.
11. A. Poater, B. Cosenza, A. Correa, S. Giudice, F. Ragone, V. Scarano and L. Cavallo, *European Journal of Inorganic Chemistry*, 2009, **2009**, 1759-1766.
12. W.-Y. Gao, Y. Chen, Y. Niu, K. Williams, L. Cash, P. J. Perez, L. Wojtas, J. Cai, Y.-S. Chen and S. Ma, *Angewandte Chemie International Edition*, 2014, **53**, 2615-2619.
13. W.-Y. Gao, L. Wojtas and S. Ma, *Chemical Communications*, 2014, **50**, 5316-5318.
14. Z.-R. Jiang, H. Wang, Y. Hu, J. Lu and H.-L. Jiang, *ChemSusChem*, 2015, **8**, 878-885.
15. O. V. Zalomaeva, A. M. Chibiryaev, K. A. Kovalenko, O. A. Kholdeeva, B. S. Balzhinimaev and V. P. Fedin, *Journal of Catalysis*, 2013, **298**, 179-185.
16. X.-Y. Li, L.-N. Ma, Y. Liu, L. Hou, Y.-Y. Wang and Z. Zhu, *ACS Applied Materials & Interfaces*, 2018, **10**, 10965-10973.
17. J. Song, Z. Zhang, S. Hu, T. Wu, T. Jiang and B. Han, *Green Chemistry*, 2009, **11**, 1031-1036.
18. T. Jing, L. Chen, F. Jiang, Y. Yang, K. Zhou, M. Yu, Z. Cao, S. Li and M. Hong, *Crystal Growth & Design*, 2018, **18**, 2956-2963.
19. B. Ugale, S. S. Dhankhar and C. M. Nagaraja, *Crystal Growth & Design*, 2018, **18**, 2432-2440.
20. F. Guo, *Journal of Molecular Structure*, 2019, **1184**, 557-561.
21. R. Srivastava, D. Srinivas and P. Ratnasamy, *Applied Catalysis A: General*, 2005, **289**, 128-134.
22. R. Babu, A. C. Kathalikkattil, R. Roshan, J. Tharun, D.-W. Kim and D.-W. Park, *Green Chemistry*, 2016, **18**, 232-242.
23. S. Senthilkumar, M. S. Maru, R. S. Somani, H. C. Bajaj and S. Neogi, *Dalton Transactions*, 2018, **47**, 418-428.
24. J. Chen, H. Li, M. Zhong and Q. Yang, *Green Chemistry*, 2016, **18**, 6493-6500.
25. M. J. Kelly, A. Barthel, C. Maheu, O. Sodpiban, F.-B. Dega, S. V. C. Vummaleti, E. Abou-Hamad, J. D. A. Pelletier, L. Cavallo, V. D'Elia and J.-M. Basset, *Journal of CO2 Utilization*, 2017, **20**, 243-252.
26. J. Lan, Y. Qu, X. Zhang, H. Ma, P. Xu and J. Sun, *Journal of CO2 Utilization*, 2020, **35**, 216-224.